scientific reports



OPEN

Optimizing toe joint stiffness to improve human-like walking

Kwonseung Cho, Kang-Woo Lee & Pilwon Hur[™]

The human metatarsophalangeal joint-often referred to as the "toe joint"-plays a vital role in gait by supporting body weight during mid-stance, enabling smooth rollover from heel to toe, and facilitating effective push-off in terminal stance. However, identifying its optimal stiffness remains challenging despite its relevance to both biological and robotic locomotion. In this study, we used a simulation-based trajectory optimization approach to investigate toe joint stiffness in a bipedal model. The results revealed that lower stiffness facilitated rollover while higher stiffness enhanced push-off. Because continuously varying stiffness is impractical in most passive devices, we extracted a single representative value (0.98 Nm/deg) by averaging the time-varying stiffness during the push-off phase. We then conducted a human walking experiment using adjustable toe joint boots across multiple stiffness conditions. The 0.98 Nm/deg condition yielded the highest subjective satisfaction and favorable spatiotemporal outcomes, especially among participants with anthropometry similar to the simulation model. Although direct numerical comparison between simulation and experiment was not performed due to modeling simplifications, key qualitative trends-such as toe joint moment progression and heel-off timing-were consistent. These findings highlight the potential of toe joint stiffness tuning to improve walking performance and user experience.

During everyday walking, the human metatarsophalangeal (MTP) joint plays a critical role in supporting a significant portion of body weight during the mid-stance phase¹. In the terminal stance phase, a natural rollover shifts the center of mass smoothly while the ankle generates sufficient force during push-off. This coordinated action-"toe joint articulation"-complements the ankle's function and is considered a crucial component of overall gait mechanics. Research on the MTP joint spans various fields, including prosthetics, footwear, sports biomechanics, wearable robotics, and humanoid robots, underscoring its significance in gait dynamics.

Previous studies on toe joints have explored two primary aspects: structural design (e.g., toe curvature) and mechanical stiffness. Honert et al.^{2,3} found that toe joint stiffness influences the push-off dynamics of the center of mass (COM), while toe shape has little effect. They also demonstrated that a longer foot arch increases COM push-off work, contributing to prosthetic and footwear design advances. McDonald et al.⁴ revealed that a flexible toe joint in a prosthetic foot reduces insertion work, whereas other parameters remain unchanged. Hong et al.⁵ reported that a 3D-printed foot with a curved toe (for the design, see⁶) enabled a more natural rollover, leading to improved consistency and symmetry in powered prosthetic walking. Furthermore, Patrick et al.⁷ observed that varying toe joint stiffness in a powered transfemoral prosthesis affects energy generation and compensatory movements, suggesting that a stiffer toe joint might reduce energy consumption in the intact limb. While both stiffness and design can influence gait mechanics, stiffness has been shown to have a more consistent and direct impact on push-off performance across studies. Design features, although relevant, tend to show context-dependent effects and typically require hardware reconfiguration, making them less suitable for systematic optimization. Accordingly, this study focuses specifically on stiffness optimization. Stiffness is a quantifiable and tunable parameter that can be implemented in both simulation and experimental settings, allowing for consistent evaluation of its biomechanical effects in a replicable framework.

In this study, we define the term "optimal toe joint stiffness" differently for simulation and experimental contexts. In the simulation, the optimal stiffness is defined as the value that minimizes the total squared joint torques (TSS), thereby representing an energetically efficient walking strategy from a purely mechanical perspective. In contrast, the experiment evaluates optimal stiffness based on user-perceived walking satisfaction as well as biomechanical indicators such as joint angles, moments, power, and stance time. This distinction is critical for interpreting the findings of this study.

Given that appropriately tuned toe joint characteristics have shown positive effects for transtibial and transfemoral amputees, it is necessary to investigate whether optimally tuned toe joint stiffness can further enhance walking performance^{4,7–9}. This study aims to identify an 'optimal' toe joint stiffness through trajectory optimization and to evaluate whether this value aligns with user preferences in human walking experiments.

Department of Mechanical and Robotics Engineering, Gwangju Institute of Science and Technology, Gwangju 61005, South Korea. [⊠]email: pilwonhur@gist.ac.kr

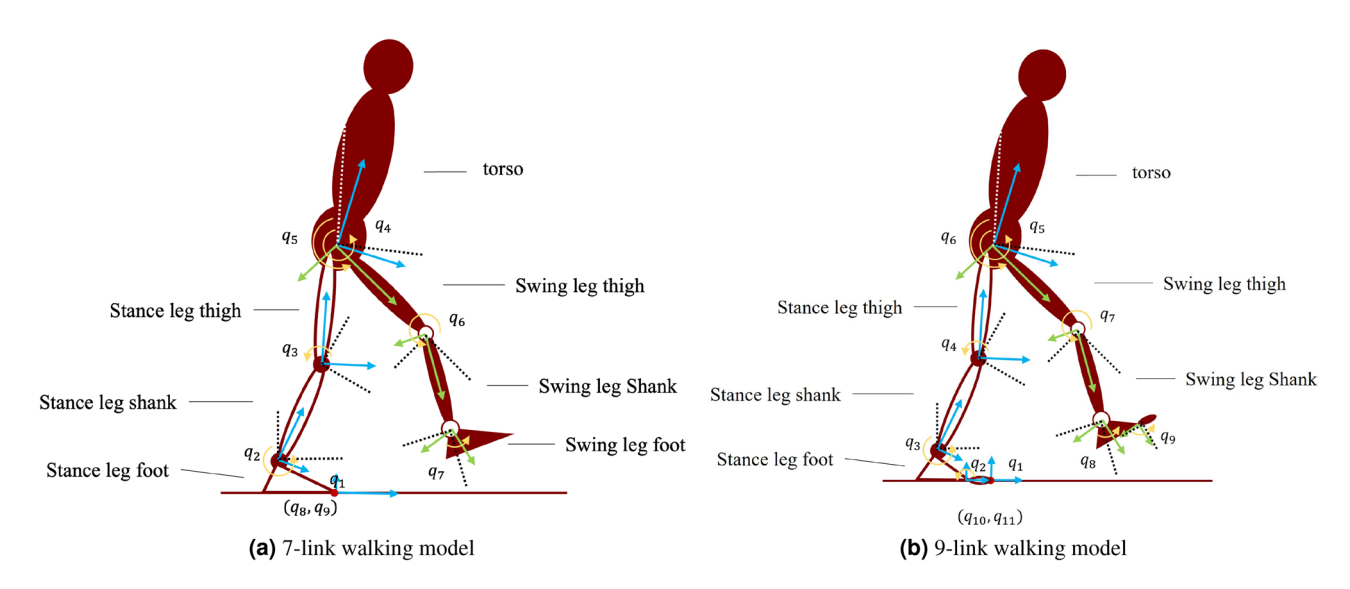


Figure 1. The schematics of the bipedal walking model for the simulation.

Name	Length (m)	Weight (kg)	
HAT	(1.000-0.530) * Height	0.678 * Weight	
Thigh	(0.530-0.285) * Height	0.100 * Weight	
Shank	(0.285-0.039) * Height	0.061 * Weight	
Foot height (7-link model)	0.039 * Height + 0.07	0.0145 * Weight+1.065	
Foot length (7-link model)	0.28		
Foot height (9-link model)	0.039 * Height + 0.07	0.0145 * Weight+0.865	
Foot length (9-link model)	0.2		
Toe	0.08	0.2	

Table 1. Details of model parameters.

To further elucidate the role of the toe joint, a trajectory optimization was performed on both a 7-link walker-serving as a baseline model without an explicit toe joint-and a 9-link walker that incorporates the toe joint. The comparison between these models helps isolate the contribution of the toe joint articulation to gait performance. To enable experimental validation, a single representative stiffness value (0.98 Nm/deg) was selected by averaging the time-varying stiffness profile during the push-off phase-where the toe joint plays a critical role in forward propulsion. Subsequently, the effects of five different toe joint stiffness levels, including this optimal value, on walking satisfaction, spatiotemporal measures, kinematics, and kinetics are analyzed. The central hypothesis is that optimized toe joint stiffness will enhance user walking satisfaction compared to non-optimized stiffness values. Section "Methods" describes the simulation method-including optimizing a 9-link bipedal model with a toe joint using the Direct Collocation Method. Section "Experiment methods" details the experimental method for validating a single optimal toe joint stiffness value, with the simulation and experimental results presented in "Results" and "Discussion", respectively.

Methods Bipedal walking model

In this study, we model bipedal walking in the sagittal plane, where the *x*-axis represents anterior-posterior displacement and the *z*-axis represents vertical displacement. Since mediolateral motion is not considered, the *y*-axis is excluded from the model. The simulation included two models: a 7-link model without toe joint, and a 9-link model that incorporates toe joints as single joints in the sagittal plane. If the toe joints in the 9-link model are assumed to have infinite stiffness, the model effectively reduces to the 7-link model. The 7-link model is depicted in Fig. 1a, while the 9-link model is shown in Fig. 1b. The detailed model parameters are described in Table 1.

Dynamic walking system

Bipedal locomotion involves a combination of continuous and discrete dynamics, which are typically modeled as hybrid systems. In this context, continuous dynamics describe the the evolution of the system state within a specific gait phase-such as initial stance, mid-stance, push-off, and swing phase -during which the foot-ground contact condition remains unchanged. Discrete dynamics, on the other hand, represent the instantaneous

transitions between these gait phases, triggered by gait events such as heel-strike, toe-strike, toe-off, and heel-off, which correspond to changes in contact configuration. Each gait phase corresponds to a distinct domain, defined by active contact constraints at specific contact points.

Continuous dynamics

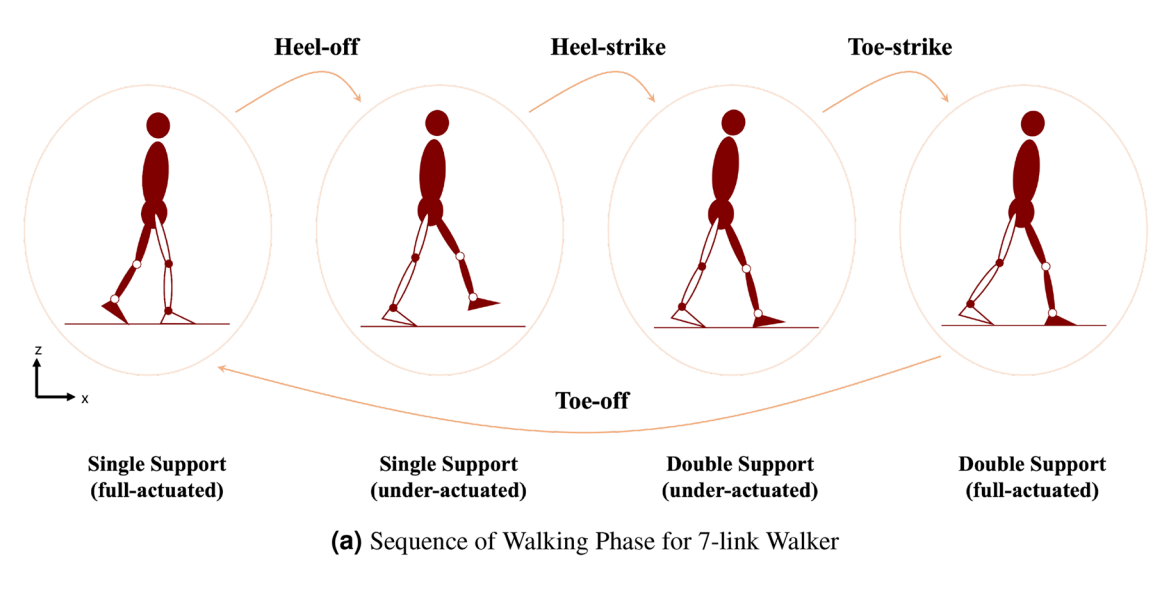
The dynamics of the rigid body walking model can be expressed as follows:

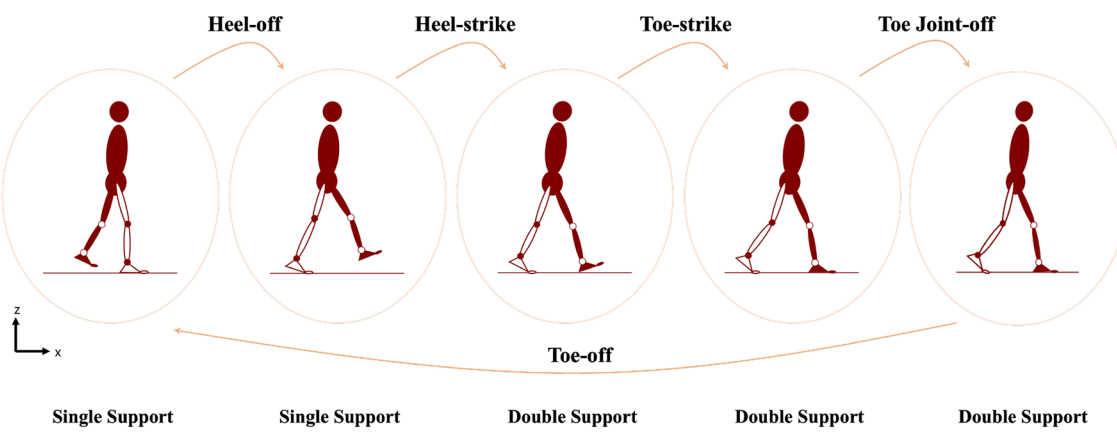
$$M(q)\ddot{q} + C(q, \dot{q})\dot{q} + G(q) = Bu + J^T F_{GRF}$$
(1)

where, $q \in Q \subset \mathbb{R}^{n \times 1}$, Q is the configuration space of a walker with n degrees of freedom, M is the inertial matrix, C includes the centrifugal and Coriolis force terms, and G is the gravity vector. B is the torque distribution matrix and u is the control input, which represents the joint torques applied at the actuated joints. D is the Jacobian matrix of the active contact point(s) D0, D1, D2, D3, and D4, D4, and D5, is the ground reaction force (GRF) vector at the active contact point(s). The position vector of any potential contact point is represented by D4, D5, where D6, and D7, where D8, are tangential and normal to the contact surface, respectively. The contact occurs when D9, reaches zero.

Discrete dynamics

During walking, discrete events occur due to changes in contact conditions with the ground, such as when a new contact is established or an existing one is changed. Two key hypotheses on contact during bipedal locomotion were made¹⁰: i) the walker configuration is invariant under impact, and ii) the collision is inelastic, and the newly created contact point remains fixed during the collision. These hypotheses are represented as reset maps that project the system from one state domain to the next (Fig. 2). The discrete dynamical equations are given by:





(b) Sequence of Walking Phase for 9-link Walker

Figure 2. The schematics of the walking sequences for the 7-link and 9-link walking model.

$$\begin{bmatrix} M & -J^T \\ J & 0 \end{bmatrix} \begin{pmatrix} \dot{q}^+ \\ \delta F_{impact} \end{pmatrix} = \begin{pmatrix} M\dot{q}^- \\ 0 \end{pmatrix}$$
 (2)

where M is the inertia matrix for the system model, including the horizontal and vertical positions of the former contact point as additional states, J is the Jacobian matrix of the active contact constraints at the contact points, δF_{impact} represents the impulse due to the collision, \dot{q}^- is the pre-impact generalized velocity, and \dot{q}^+ is the post-impact generalized velocity.

Walking sequence from human data

Once a stable periodic gait is achieved, the sequence of walking phases becomes fixed and repeats cyclically. This allows for the use of a predefined contact sequence in hybrid trajectory optimization. In this study, we utilize the contact sequence shown in Fig. 2, which closely reflects the pattern observed in typical human walking.

Optimization process for dynamic walking system

We introduce the method of trajectory optimization using the direct collocation 11,12 for hybrid systems with multiple domains. The direct collocation method is a numerical optimization technique that discretizes the equations of motion at multiple collocation points, transforming a continuous optimal control problem into a nonlinear programming problem for efficient trajectory optimization. The contact sequence and associated domains are shown in Fig. 2. The general optimization formula for direct collocation is given as follows:

$$x^* = \operatorname{argmin}_{x} J(x)$$
s.t. $x_{lb} \le x \le x_{ub}$

$$H_{eq}(x) = 0$$

$$H_{iq}(x) \ge 0$$
(3)

where, the system consists of N domains and M collocation points, with the decision variable \mathbf{x} defined as $\mathbf{x} = [q_i, \dot{q}_i, \ddot{q}_i, u_i, F_{GRF_i}, \delta F_{impact}, \Delta t_n]$ for $i \in [1, 2, \cdots, M]$ and $n \in [1, 2, \cdots, N]$. \mathbf{x}_{lb} and \mathbf{x}_{ub} represent the lower and upper bounds for \mathbf{x} , while $H_{eq}(\mathbf{x})$ and $H_{iq}(\mathbf{x})$ denote the equality and inequality constraints, respectively. The objective is to minimize $J(\mathbf{x})$ while satisfying all constraints.

Hermite simpson collocation

In our direct collocation approach, we utilize the Hermite-Simpson method to discretize all joint variables q, \dot{q} , and \ddot{q} as nodes of cubic splines. The Hermite-Simpson constraint (H_{HSM}) relates the states between adjacent collocation points k-1 and k+1 (with k being an even number) within domain n, and is defined as follows:

$$x_{k} - \frac{1}{2}(x_{k+1} + x_{k-1}) - \frac{1}{8}\Delta t_{n}(\dot{x}_{k-1} - \dot{x}_{k+1}) = 0$$

$$x_{k+1} - x_{k-1} - \frac{1}{6}\Delta t_{n}(\dot{x}_{k-1} + 4\dot{x}_{k} + \dot{x}_{k+1}) = 0$$
(4)

where $\mathbf{x}_k = [q_k, \dot{q}_k]^T$ and Δt_n is the time step in domain n.

Cost function for dynamic walking

Zarrugh et al. ¹³ noted that within the normal walking speed range, there exists a unique speed for a given step length that minimizes energy consumption, and humans naturally adopt this energy-efficient walking pattern. Motivated by this, we base our cost function on overall effort, computed via the sum of squared torques (TSS). Although the Cost of Transport (COT) more directly reflects metabolic energy, TSS offers a simpler yet sufficiently robust measure of effort, facilitating stable convergence in our trajectory-optimization framework. Simpson's quadrature rule is then applied to integrate TSS over each domain *n*, as outlined below.

$$J_{n}(\mathbf{x}) = \sum_{j=1}^{M_{n}} \omega_{j} u_{j}^{2}$$

$$\omega_{j} = \begin{cases} \frac{1}{9} \Delta t_{n} & \text{if } j = 1 \text{ or } j = M_{n} \\ \frac{1}{3} \Delta t_{n} & \text{if } j \text{ is even} \\ \frac{1}{3} \Delta t_{n} & \text{else} \end{cases}$$
(5)

In this context, Δt_n represents the time step in the domain n, corresponding to the time interval between the collocation points k-1 and k+1 in Eq. (4). M_n , an odd integer, denotes the number of collocation points in domain n (where $n \in [1, 2, \ldots, N]$). The total cost is then computed accordingly.

$$J(x) = \frac{1}{mg} \sum_{n=1}^{N} J_n(x)$$
 (6)

where mg is the walker's weight.

Constrained dynamics

In trajectory optimization, general constraints are crucial. The direct collocation method requires setting bounds for each decision variable, such as joint positions, torques, and ground reaction forces, based on the range of motion for each joint. The constrained dynamics for the system are expressed as Eq. (7):

$$M(q)\ddot{q} + C(q,\dot{q})\dot{q} + G(q) - Bu - J^T F_{GRF} = 0$$

 $J\ddot{q} + \dot{J}\dot{q} = 0$ (7)

where $F_{\rm GRF}$ is the ground reaction forces at the active contact point(s), and all other symbols are defined as in Eq. (1). The second equation in Eq. (7) ensures that the floating model is supported by the ground at the contact points.

Contact constraints

To model contact conditions, additional constraints are introduced to account for the ground reaction forces and friction at the ground. The friction cone model, based on Coulomb friction, ensures that the contact forces remain within acceptable limits:

$$\mu F_{\text{GRF},z} - |F_{\text{GRF},x}| \ge 0$$

$$\phi_z(q) = 0$$

$$J\dot{q} = 0$$
(8)

where μ is the friction coefficient, $F_{\text{GRF},x}$ is the horizontal contact force, $F_{\text{GRF},z}$ is the normal contact force, and $\phi_z(q)$ is the normal distance from the contact point to the contact surface. $J\dot{q}=0$ ensures that the contact point is stationary.

Boundary constraints

Boundary constraints manage the transition of states between different domains as contact conditions change. These constraints are similar to those described in discrete dynamics:

$$M(q^{-})(\dot{q}^{+} - \dot{q}^{-}) - J^{T} \delta F_{impact} = 0$$

$$q^{+} - q^{-} = 0$$
(9)

where the superscript "+" denotes the post-impact state, the superscript "-" denotes the pre-impact state.

Continuity constraints

Continuity constraints ensure that the trajectory remains cyclic and smooth by connecting the start and end points of the trajectory:

$$R(q_{start}) - q_{end} = 0$$

$$M(q_{end})(R(\dot{q}_{start}) - \dot{q}_{end}) - J^T \delta F_{impact} = 0$$

$$x_{com}(q_{end}) - x_{com}(q_{start}) \ge d_{dim}$$
(10)

where R is the relabeling matrix to swap joint variables between legs and d_{min} is the minimum horizontal traveling distance of the center of mass position x_{com} . These constraints are essential for maintaining the integrity and feasibility of the optimized trajectory.

Simulation environment

The simulation environment is described in Table 1, detailing the model parameters, including a total height of 1.83~m and a mass of $80~kg^{14}$. We utilized JuMP (v1.22.2) in Julia (v1.10.4) for modeling and employed IPOPT (v1.6.3) as the nonlinear programming solver 15 . The equations of motion and constraints were formulated using HurToolbox (v2.0.5), a custom robotics package for Mathematica (v12, Wolfram, Champaign, IL), and automatic differentiation was employed to compute the Jacobian matrices. All simulations were conducted on a MacBook Pro M1.

Computation of toe joint stiffness from optimized trajectories

Following trajectory optimization, we obtained time-resolved profiles of toe joint angle and torque throughout the gait cycle. Toe joint stiffness corresponds to the slope of the torque-angle relationship; thus, at each time step, the toe joint stiffness was computed by taking the ratio of torque to angle. This yielded a time-varying stiffness profile that reflects how the joint behaves dynamically across different gait phases. To facilitate experimental validation, we focused on the push-off phase-where the toe joint contributes most significantly to propulsion-and determined the representative slope for this interval by solving a least-squares problem on the stiffness values. This average slope was then used as the fixed stiffness setting for comparison across experimental conditions.

Sensitivity analysis method

To evaluate the robustness of the optimization framework to anthropometric variation, we conducted sensitivity analyses on both body height and mass. For height, we varied the model from 162 to 183 cm in 2–3 cm

increments, while keeping mass fixed at $80 \, kg$. Conversely, in the mass perturbation test, we varied mass from 75 kg to $85 \, kg$ while fixing height at $183 \, \text{cm}$.

For each simulation, we assessed whether the optimization converged, and if so, recorded the resulting values of the cost function, step length, and walking speed. Sensitivity coefficients were calculated using the following formula:

$$S = \frac{\Delta y/y_0}{\Delta x/x_0}$$

where Δy and Δx represent changes in the output and input values, respectively, and y_0 , x_0 are their corresponding baseline values. These coefficients quantify how responsive the outputs are to changes in input parameters, with lower values indicating higher robustness.

Experiment methods

An experimental method was employed to evaluate the effect of the optimal toe joint stiffness. The average stiffness value during the push-off phase-where the toe joint plays the most significant role in the gait cycle-was calculated to validate the optimization results for the toe joint stiffness profile. This process yielded a passive toe joint stiffness value of **1.04 Nm/deg**. A pair of simulated shoes with a passive toe joint was designed, as shown in Fig. 3. A cantilever spring made of 1095 spring steel was used to replicate the passive toe joint, with varying stiffness achieved by altering spring thickness. The overall length of each prosthetic foot was **28 cm** from heel to toe, and the heel-to-MTP-axis distance was **20 cm**, mirroring average human-foot anthropometrics reported in the literature². These geometric constraints ensure that the adjustable toe joint operates about the same anatomical location and lever arm as the biological joint, thereby reproducing realistic joint kinematics and kinetics. The experimental setup included nine motion capture cameras (Nokov Mars, Beijing, China) and a 6-meter-long instrumented flat ground with a force plate (AMTI BMS400600-2000, MA, USA).

Toe joint stiffness selection

Simulation (see Result) identified the optimal toe joint stiffness as 1.04 Nm/deg. Several experimental stiffness values were selected to validate this in a human walking context. The closest achievable stiffness with a cantilever spring was 0.98 Nm/deg (3.5T spring). The selected experimental variables included 0.56 Nm/deg (2T), 0.98 Nm/deg (3.5T), and 1.4 Nm/deg (5T). Two extreme conditions were also tested: 0 Nm/deg and infinite stiffness (rigid body). It is important to clarify that the 0 Nm/deg condition does not imply the absence of a toe joint; instead, when the foot length is fixed at 280 (e.g., mm), the 0 Nm/deg condition indicates that the toe joint is present but provides no resistance. In contrast, the infinite stiffness condition represents a scenario in which the toe joint behaves as a rigid body, effectively functioning as if the toe joint were absent. The experimental conditions tested were 0 Nm/deg, 0.56 Nm/deg, 0.98 Nm/deg, 1.4 Nm/deg, and infinite stiffness.

Subjects

Twenty healthy, able-bodied subjects (10 males, 10 females; age: 25.75 ± 4.2 years; weight: 56.9 ± 8.7 kg; height: 1.66 ± 7.4 m) participated in a gait analysis study. All participants provided written informed consent, and the Institutional Review Board of the Gwangju Institute of Science and Technology provided approval for this study (20230615-HR-EX-002). All methods were performed in accordance with the relevant guidelines and regulations.



Figure 3. Adjustable toe joint simulation boots.

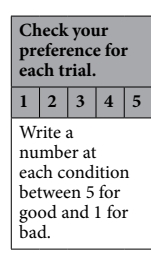


Table 2. Preference survey.

Model	Objective value	Step length	Walking speed	Walking time
7-Link Walker	2.06×10^{7}	0.61 m	0.86 m/s	0.7 s
9-Link Walker	8.41×10^{6}	0.68 m	1.07 m/s	0.63 s

Table 3. 7-link walker and 9-link walker comparison.

Protocol

Training session

Prior to the experiment, each subject practiced walking on a flat surface while wearing the simulation boots to acclimate to the device. The training session, conducted on a treadmill, lasted a minimum of 5 minutes. Subjects were allowed to request to end the session once they felt their gait was stable. Although the training session did not include scheduled breaks, sufficient rest was allowed upon request. The practice session was repeated for all five toe joint stiffness conditions, with the session restarting each time the stiffness was changed. During the session, a researcher followed one or two steps behind the subject to ensure safety and prevent falls.

Data collection

After a 5-minute break following the training session, the test session was conducted. Subjects wore the simulation boots and walked on a 6-meter-long flat surface equipped with a force plate. Markers were attached to the lower limbs to analyze joint movements. The test session was conducted for all toe joint stiffness conditions (0, 0.56, 0.98, 1.4, and infinite Nm/deg) in a randomized order. For each condition, subjects completed ten walking trials at a self-selected comfortable speed.

User preference surveys on toe joint stiffness were conducted after each test session for each experimental condition. The survey procedure was explained to each subject before the test began. After completing the session for each stiffness condition, subjects were given a 5-minute break, during which a 5-point Likert scale survey was administered to assess gait preference. The simulation boot were then switched to a different toe joint stiffness in a randomized order. To avoid bias, specific details of the experimental variables were not disclosed to the subjects. The preference survey is shown in Table 2.

Data processing

Post-processing of the data was conducted using Nokov (Nokov, Beijing, China) and Visual3D software (C-Motion, Germantown, MD, USA). Marker trajectories, and force data were filtered in Visual3D using a low-pass fourth-order butter worth filter at 5 and 10 Hz, respectively. Visual3D was also used to calculate hip, knee, ankle, and toe joint angles, moments, and power. Additionally, marker and force data were utilized to determine walking and push-off times. All statistical analyses were performed using R-Studio. For all kinetic, kinematic, and spatiotemporal parameters, values were reported as mean \pm standard deviation (SD) For normally distributed data, a one-way repeated-measures ANOVA was conducted with significance level set at $\alpha=0.05$. When significant effects were found, Tukey's post-hoc test was applied for pairwise condition comparisons. For user preference scores, which did not meet the assumptions of normality, a Kruskal-Wallis test was used. Specifically, for gait preference data, a Friedman test was conducted, followed by Wilcoxon signed-rank tests for paired comparisons with Bonferroni correction. All statistical results were considered significant at p < 0.05

Results

Simulation results

7-link walker vs. 9-link walker

To compare the bipedal models with and without the toe joint, the optimization results of the 7-link and the 9-link walking models were analyzed. The objective value for the 7-link model was higher (2.06×10^7) than for the 9-link model (8.41×10^6) . While step lengths were similar between the two models, the walking speed was faster in the 9-link model, which includes toe joints. These results are summarized in Table 3.

Sensitivity analysis results

As summarized in Table 4, the optimization remained stable and convergent across all height variations (183–162 cm), with moderate changes in outputs. Relative changes were 4.2% for cost, 5.9% for step length, and

Metric	Min	Max	Relative change (%)	Sensitivity coefficient
Optimization cost (×10 ⁶)	8.07	8.42	- 4.2%	0.36
Step length (m)	0.64	0.68	- 5.9%	0.51
Walking speed (m/s)	0.98	1.07	- 8.4%	0.73

Table 4. Sensitivity analysis for height variation (mass fixed at 80 kg).

8.4% for walking speed, and sensitivity coefficients were below 0.75 in all cases, indicating strong robustness to geometric changes.

In contrast, for mass perturbations, the optimization failed to converge for all tested values $(75-85 \ kg)$, even though the changes were relatively small (\pm 6%). These failures suggest that the model is highly sensitive to mass-driven dynamics such as torque demand and contact forces, and that the current formulation does not generalize well to varying body mass.

Domain-specific simulation of toe joint dynamic

The simulation consists of five domains spanning from left toe-off (LTO) to right toe-off (RTO), covering the stance phase of the right leg. Figure 4 illustrates the time-varying profiles of toe joint angle, torque, and stiffness throughout the stance phase.

In Domain 1 (LTO to RHO), the toe joint angle remains nearly constant at zero, resulting in very high stiffness due to zero angular displacement, as the right foot fully supports the body weight. In Domain 2 (RHO to LHS), the toe joint begins to dorsiflex, but torque remains low, leading to a rapid drop in stiffness, indicating a transition toward rollover. In Domain 3 (LHS to LTS), the toe continues dorsiflexing while torque remains minimal, resulting in sustained low stiffness, facilitating a smooth rollover of the center of mass. In Domain 4 (LTS to RTJO), both angle and torque gradually increase, causing toe joint stiffness to rise, which assists propulsion. In Domain 5 (RTJO to RTO), the toe angle reduces slightly while torque peaks, resulting in a sharp increase in stiffness, enabling efficient push-off and energy transfer. The average stiffness computed across Domain 5-where the toe joint plays a dominant role in late push-off-was approximately 1.04 Nm/deg.

Experimental results

Joint angles, moments, and powers

The experimental results were divided into two groups based on height. Group 1 consisted of participants taller than 175 cm, similar to the simulation model, while Group 2 included participants shorter than 175 cm. The results for joint angles, moments, and power are shown in Fig. 5.

In both groups, the toe joint exhibited distinct kinematic and kinetic responses depending on the stiffness condition. The largest dorsiflexion angle was observed in the 0 Nm/deg condition, while the 0.56 Nm/deg condition exhibited the second largest dorsiflexion angle. Additionally, the 0.98 Nm/deg and 1.4 Nm/deg conditions showed the smallest and similar ranges of dorsiflexion. Statistically significant differences were found between the 0 Nm/deg condition and all other conditions (p < 0.05). Furthermore, significant differences were observed between the 0.56 Nm/deg and 0.98 Nm/deg conditions and between the 0.56 Nm/deg and 1.4 Nm/deg conditions (p < 0.05). In contrast, the moment and power results showed an inverse trend. The 1.4 Nm/deg condition produced the highest peak moment at maximum dorsiflexion, which was statistically significant compared to the other two conditions (p < 0.05). The 0.98 Nm/deg and 0.56 Nm/deg conditions tended to follow in peak moment size, though there was no statistical difference.

Despite these notable differences at the toe joint, both groups displayed generally similar ankle kinematics and kinetics across most stiffness conditions. The sole exception was the 0 Nm/deg condition-which, although it includes a toe segment, effectively provides no resistance-leading to a significantly reduced ankle dorsiflexion angle (p < 0.05). Additionally, knee and hip joint measurements showed no significant differences among the experimental stiffness levels, suggesting that the presence or absence of toe joint resistance did not substantially influence proximal joint mechanics.

Spatiotemporal parameters

Figure 6 presents the spatiotemporal parameter rushs. In the pooled dataset combining Group 1 and Group 2 (Total), stance time differed significantly across toe joint stiffness conditions. Specifically, the 0 Nm/deg condition showed significantly shorter stance time compared with the 0.56 Nm/deg, 1.4 Nm/deg, and ∞ Nm/deg conditions (p<0.05). In Group 1, a significant difference was found only between the 0 Nm/deg and ∞ Nm/deg conditions, whereas in Group 2, the 0 Nm/deg condition was significantly shorter than both the 1.4 Nm/deg and ∞ Nm/deg conditions (p<0.05). No significant differences were observed for swing time, stride length, walking time, or walking speed, although stride length showed a non-significant trend toward reduction with increasing stiffness.

Figure 7 presents the heel-off timing results for the pooled dataset alongside findings from Group 1 and Group 2. In the pooled dataset, the earliest heel-off occurred under the 0 Nm/deg condition; as toe joint stiffness increased, heel-off timing was progressively delayed. Statistical results for Heel-off timing are presented in Table 5. In the Total group, the 0 Nm/deg condition exhibited significantly earlier heel-off compared with the 0.98 Nm/deg, 1.4 Nm/deg, and ∞ Nm/deg conditions (p < 0.05), and the 0.56 Nm/deg and 0.98 Nm/deg conditions were also significantly different from ∞ Nm/deg. In Group 1 (over 175 cm), the 0 Nm/deg condition was significantly different from all other stiffness conditions (p < 0.05), indicating the earliest heel-off timing.

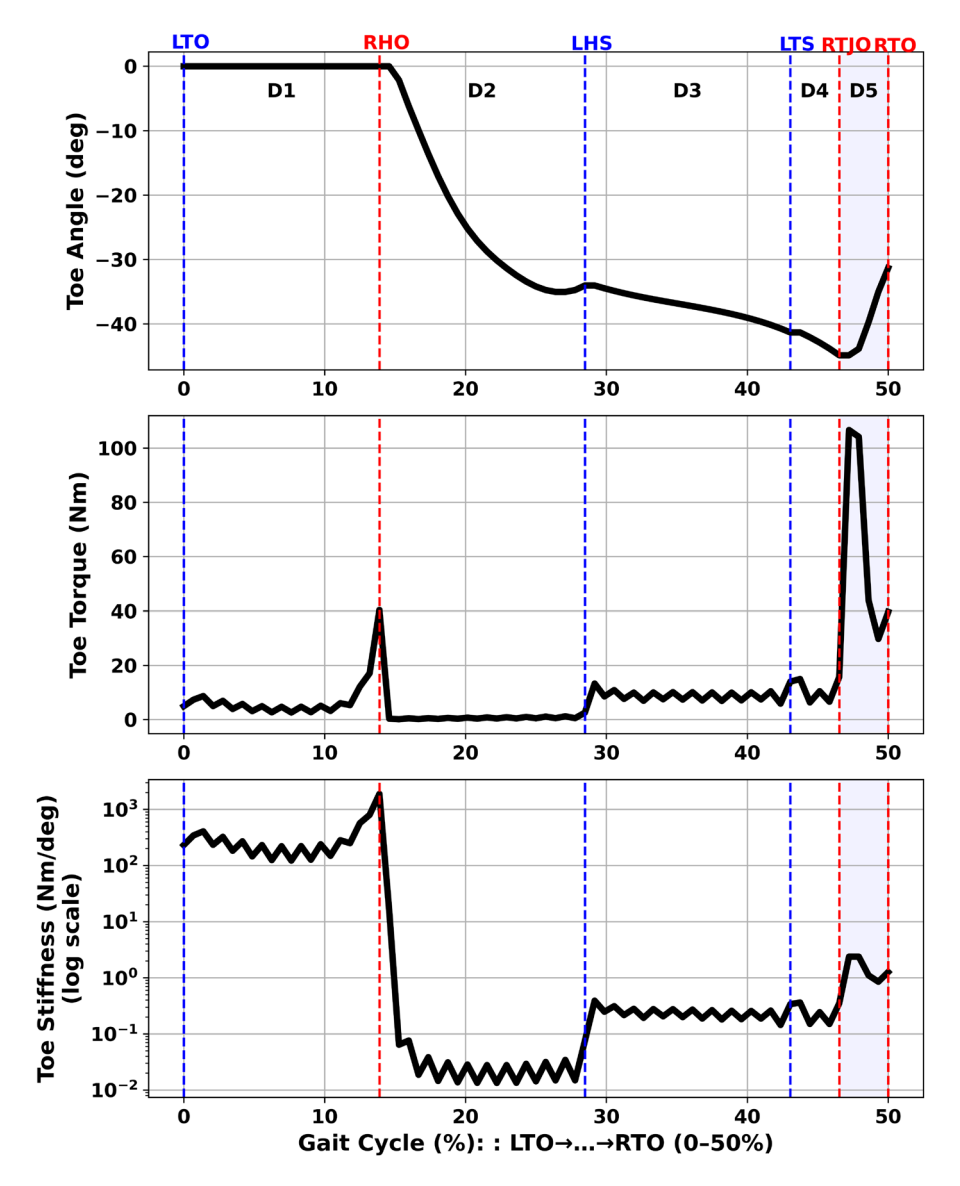


Figure 4. Toe joint biomechanics during the stance phase of the gait cycle. From top to bottom: toe joint angle (deg), torque (Nm), and stiffness (Nm/deg, log scale) plotted against normalized gait cycle percentage. Colored dashed lines indicate gait events: left toe-off (LTO), right heel-off (RHO), left heel-strike (LHS), left toe-strike (LTS), right toe-joint-off (RTJO), right toe-off (RTO). Each domain (1–5) corresponds to a distinct sub-phase. Domain 1 exhibits near-infinite stiffness due to static toe posture; Domains 2 and 3 reflect a rollover phase with low stiffness; Domains 4 and 5 show increasing stiffness to support propulsion and push-off.

In Group 2 (under 175 cm), significant differences were observed between 0 Nm/deg and ∞ Nm/deg, as well as between 0.56 Nm/deg and ∞ Nm/deg.

Gait preference

The overall preference results differed between the two groups, as shown in Fig. 8. In Group 1 (participants 175 cm or taller), similar to the robot model, the preferences ranked as follows: 0.98, 0.56, 1.4, 0, and infinite Nm/deg, with average scores of 4.3 ± 0.823 , 3.9 ± 0.316 , 3.4 ± 0.843 , 2.9 ± 1.197 , and 1.7 ± 0.483 , respectively. Within this group, the 0.56 Nm/deg and 0.98 Nm/deg conditions each showed significantly higher preference ratings compared with the ∞ Nm/deg condition (p < 0.05). In Group 2 (participants shorter than 175 cm) exhibited a different preference order: 0, 0.98, 0.56, 1.4, and infinite Nm/deg, with average scores of 4.3 ± 0.949 , 3.5 ± 0.527 , 3.1 ± 0.738 , 2.8 ± 0.421 , and 1.6 ± 0.966 , respectively. In this group, only the 0.98 Nm/deg condition was rated significantly higher than ∞ Nm/deg (p < 0.05). Across both groups, the 0.98 Nm/deg condition consistently achieved the highest or near-highest preference scores, indicating a strong user preference for moderate toe joint stiffness. In contrast, the ∞ Nm/deg condition received the lowest scores in both groups, suggesting that very high stiffness is generally unfavorable to users.

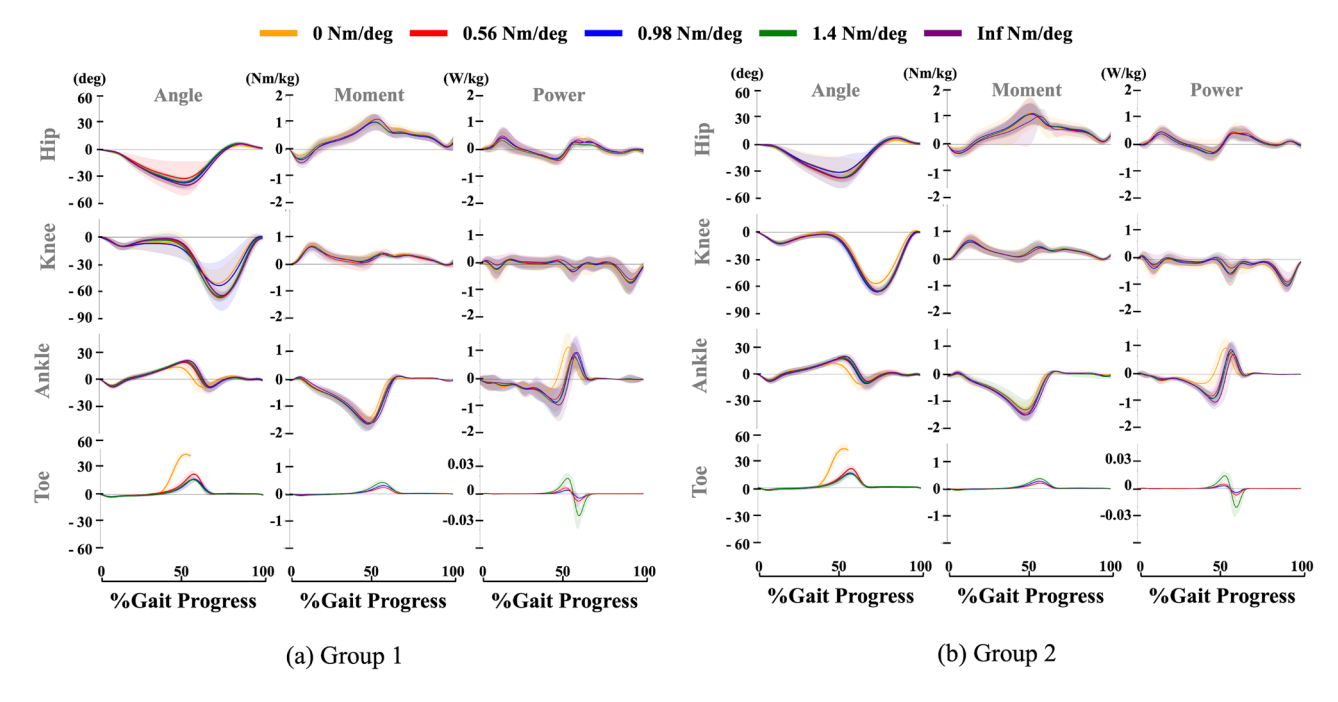


Figure 5. Joint Angle, Moment, and Power results (a) Group1 (under 175 cm). (b) Group2 (over 175 cm). The 0 Nm/deg condition represents simulation boots without a toe joint; in other words, while the toe joint is present, it provides no resistance. Therefore, in the toe joint angle graph, the 0 Nm/deg condition data exist only until the toe joint is off.

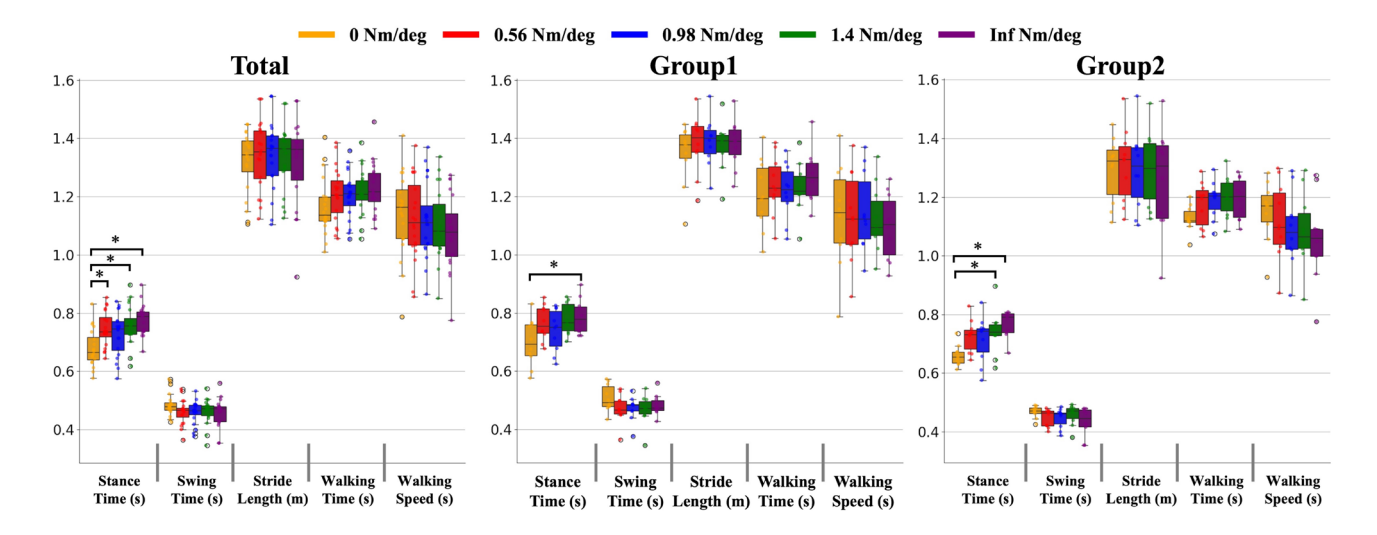


Figure 6. Spatiotemporal gait parameters across five toe joint stiffness conditions (0, 0.56, 0.98, 1.4, and Inf Nm/deg) for all participants (Total), Group 1, and Group 2. Parameters include stance time, swing time, stride length, walking time, and walking speed. Asterisks (*) denote statistically significant pairwise differences (p < 0.05).

Discussion

In this study, the term "optimal stiffness" is defined contextually in both the simulation and experimental frameworks. In the simulation, optimal stiffness refers to the value that minimizes total squared joint torques (TSS), representing an energetically efficient trajectory under physical constraints. In contrast, the experimental definition of optimal stiffness incorporates subjective walking satisfaction and biomechanical metrics such as toe joint angle, torque, power, and stance time. While the two definitions differ, we evaluate how closely the simulation-based optimal value aligns with participants' actual preferences.

In this study, we aim to determine whether the trajectory optimization technique can identify the 'optimal' stiffness of the toe joint and verify whether this stiffness aligns with participants' preferences, after walking in a simulation foot. The optimization process yielded an optimal toe joint angle and torque trajectory. The

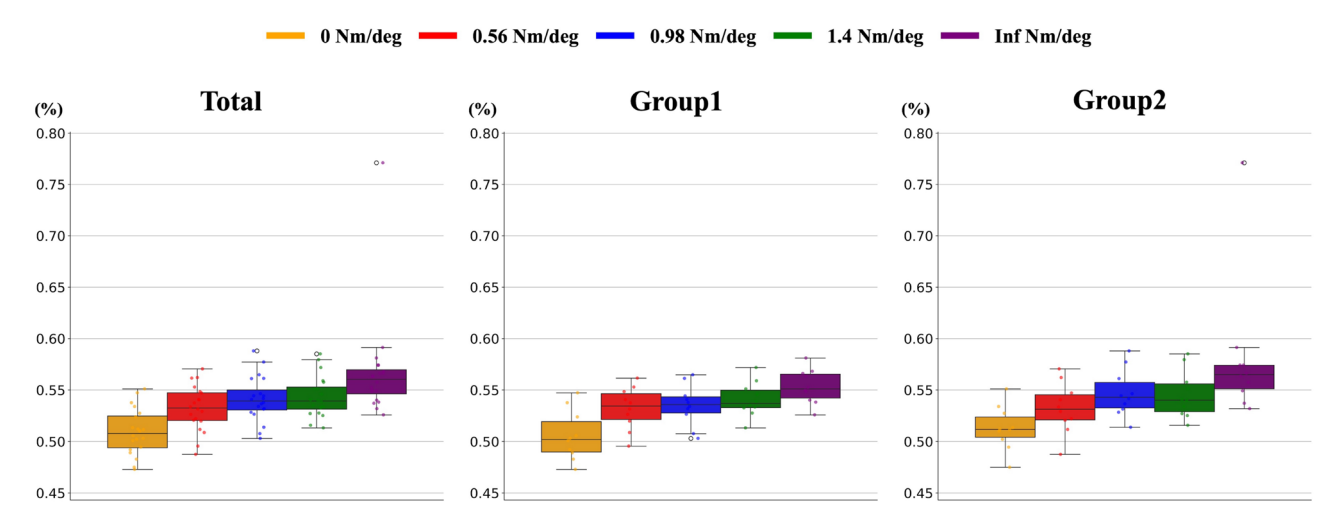


Figure 7. Heel-off timing (% gait cycle) across five toe joint stiffness conditions (0, 0.56, 0.98, 1.4, and Inf Nm/deg) for all participants (Total), Group 1, and Group 2. Boxplots display the median (central line), interquartile range (box), whiskers (1.5×IQR), and individual data points, illustrating changes in heel-off timing distribution with varying toe joint stiffness.

	0 Nm/deg	0.56 Nm/deg	0.98 Nm/deg	1.4 Nm/deg	∞ Nm/deg			
Total (all participants)								
0 Nm/deg	-	0.1102	0.0092**	0.0044**	< .0001***			
0.56 Nm/deg	-	-	0.8878	0.7764	0.0029**			
0.98 Nm/deg	-	-	-	0.9993	0.0459*			
1.4 Nm/deg	-	-	-	-	0.0823			
∞ Nm/deg	-	-	-	-	-			
Group 1 (over	Group 1 (over 175 cm)							
0 Nm/deg	_	0.0307*	0.0128*	0.0020**	< .0001***			
0.56 Nm/deg	-	-	0.9973	0.8637	0.1356			
0.98 Nm/deg	-	-	-	0.9666	0.2545			
1.4 Nm/deg	-	-	-	-	0.6207			
∞ Nm/deg	-	-	-	-	-			
Group 2 (under 175 cm)								
0 Nm/deg	-	0.7666	0.2621	0.2987	0.0013**			
0.56 Nm/deg	_	-	0.9058	0.9312	0.0361*			
0.98 Nm/deg	-	-	-	1.0000	0.2367			
1.4 Nm/deg	-	-	-	-	0.2055			
∞ Nm/deg	-	-	-	-	_			

Table 5. Pairwise comparison p-values for heel-off timing (% gait cycle) across five toe joint stiffness conditions. Significant differences are denoted by * (p < 0.05), ** (p < 0.01), and *** (p < 0.001).

comparison between the 7-link and 9-link models reveals essential differences: the 9-link model, which includes toe joints, exhibits a longer stride length and faster walking speed than the 7-link model. Additionally, the 9-link model has a lower objective value, indicating that less overall torque is required when toe joints are present. Therefore, the inclusion of toe joints significantly impacts the torque demands in bipedal locomotion.

The contrast between the height and mass sensitivity results highlights a key characteristic of the model: it is structurally robust but dynamically sensitive. While height changes-representing geometric variation-produced stable and convergent results, even minor changes in mass led to optimization failure. This suggests that the contact and actuation constraints are tightly coupled with mass-dependent dynamics.

The bipedal model's toe joint behavior was analyzed across five domains in the simulation. In Domain 1, the mid-stance phase where the stance foot supports most body weight, the toe joint exhibited infinite stiffness due to zero angular displacement, ensuring a stable support base. Infinite stiffness resulted from the zero angular displacement of the toe joint. These results are consistent with the previous clinical study indicating that toes are critical in increasing the weight-bearing area during walking¹. In Domain 2, as the the stance heel lifted off, the toe joint showed zero stiffness, facilitating a natural rollover. In Domain 3, the early phase of the double support,

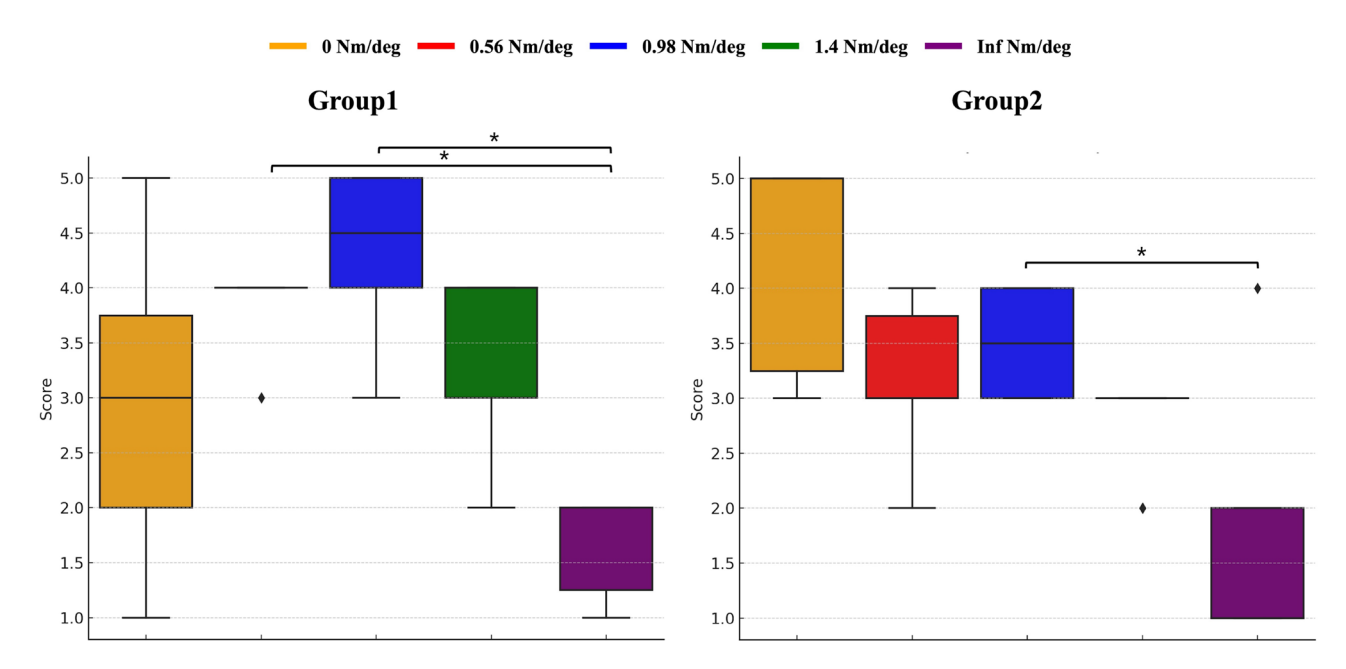


Figure 8. Gait Preference socres by group across five toe joint stiffness conditions (0, 0.56, 0.98, 1.4, and Inf Nm/deg) for Group 1, and Group 2. ♦ denote outliers; Asterisks (*) denote statistically significant pairwise differences (p < 0.05).

the stiffness initially increased to absorb the opposite foot's heel strike, then gradually converged to near-zero for a smooth rollover. In Domain 4, the early push-off phase, the stiffness gradually increased from near-zero, aiding propulsion. Lastly, in Domain 5, the late push-off phase from toe-joint-off to toe-off, the stiffness sharply increased as the toe joint left from the ground, enabling efficient energy transfer and momentum generation. The simulation results align with the intuitive role of the toe joint in human locomotion, confirming the feasibility of the optimal solution.

According to Fig. 5, The simplified experimental results for the toe joint were consistent across both groups. The moment results aligned with previous studies¹, showing that as toe joint stiffness increases, the anterior center of pressure extends further, generating greater toe joint moments. An interesting observation was made in the joint angles and power analysis: the largest dorsiflexion angle occurred at 0.56 Nm/deg, whereas similar dorsiflexion ranges were noted at 0.98 Nm/deg and 1.4 Nm/deg. The peak power was highest at 1.4 Nm/deg, with slightly lower but comparable levels at 0.98 Nm/deg and 0.56 Nm/deg. If rollover and push-off, as indicated by the toe joint's angle and power trends, are the key gait events, then 0.56 Nm/deg suggests easier rollover, while 1.4 Nm/deg provides stronger push-off assistance. Thus, 0.98 Nm/deg appears to offer a balance between ease of rollover and push-off assistance.

According to Fig. 5, The ankle joint results were also consistent across both groups. In the 0 Nm/deg condition, participants exhibited shorter stance times and faster rollover due to the reduced support base, limiting dorsiflexion as ankle stiffness increased. While ankle moments did not significantly differ across conditions, the smallest peak dorsiflexion angle was observed in the 0 Nm/deg condition. Previous studies have shown that reduced peak dorsiflexion at the ankle can alter lower limb movement patterns during gait, potentially weakening forward propulsion and increasing the risk of injury^{17–20}. According to Fig. 5, The kinematic and kinetic results for the knee and hip joints showed no significant differences among the experimental conditions, suggesting that the presence or absence of the toe joint did not impact their gait patterns.

In the analysis of spatiotemporal parameters (Fig. 6), significant differences in stance time were observed in the Total dataset between the 0 Nm/deg condition and the 0.56 Nm/deg, 1.4 Nm/deg, and ∞ Nm/deg conditions (p < 0.05). In Group 1, a significant difference was found only between 0 Nm/deg and ∞ Nm/deg, while in Group 2, 0 Nm/deg was significantly shorter than both 1.4 Nm/deg and ∞ Nm/deg. Across all cases, the 0 Nm/deg condition exhibited the shortest stance time, suggesting that greater toe flexibility shortens the stance phase. This may be because increased mobility reduces anterior center of pressure progression time, allowing a smoother rollover and push-off. No significant differences were found in other spatiotemporal parameters (i.e., swing time, step length, stride length, walking time, walking speed) $^{21-24}$.

According to the heel-off timing results (Fig. 7), increasing toe joint stiffness systematically postponed heel-off. In the Total dataset, 0 Nm/deg showed earlier heel-off than 0.56 Nm/deg, 1.4 Nm/deg, and ∞ Nm/deg, while in Group 1, a significant difference was found only between 0 Nm/deg and ∞ Nm/deg, and in Group 2, between 0 Nm/deg and 1.4 Nm/deg and between 0 Nm/deg and ∞ Nm/deg. In 0 Nm/deg, heel-off occurred near 50% of the gait cycle, closely matching typical human walking patterns and indicating that greater toe flexibility supports a more natural rollover motion. In contrast, higher stiffness delayed heel-off, potentially reducing gait naturalness. These findings highlight that moderate toe joint flexibility can better mimic human biomechanics and may improve rollover smoothness during walking.

According to Fig. 8, preference results indicated that moderate toe joint stiffness was generally favored across participants. In both groups, the 0.98 Nm/deg condition received the highest or near-highest ratings, while the ∞ Nm/deg condition consistently had the lowest scores, suggesting that excessive stiffness limits natural gait patterns and reduces comfort. Statistically, in Group 1, both the 0.56 Nm/deg and 0.98 Nm/deg conditions were preferred significantly more than ∞ Nm/deg, whereas in Group 2, only the 0.98 Nm/deg condition showed a significant advantage over ∞ Nm/deg. The taller group favored values close to the assumed optimal stiffness (0.98 Nm/deg), while the shorter group preferred 0 Nm/deg. Considering that average height correlates with foot size, the shorter group's preference for 0 Nm/deg may relate to foot size, as they felt more satisfied with the shorter footplate. Both groups showed the lowest preference for the ∞ Nm/deg condition, indicating discomfort when the toe joint did not bend. These results highlight that while the absolute ranking of stiffness preferences varied somewhat between groups, the negative perception of very high stiffness was consistent. This finding underscores the importance of avoiding excessive stiffness in toe joint design and prioritizing stiffness ranges that maintain foot rollover and perceived comfort.

The comprehensive experimental results indicate that the toe joint's optimal stiffness should ideally vary according to each phase of the gait cycle. Specifically, maintaining low stiffness (0 Nm/deg) during heel-off and rollover promotes a smoother transition, whereas employing a higher stiffness in push-off enhances propulsion efficiency. Thus, instead of being treated as a single fixed value, the toe joint's stiffness is best conceptualized as a time-varying parameter that adapts dynamically. Nonetheless, when considering a single stiffness value, 0.98 Nm/deg proves most beneficial for enhancing walking satisfaction. This value was strongly preferred by taller participants and ranked second among shorter participants, closely aligning with the simulation-derived optimum of 1.04 Nm/deg. The broad applicability of 0.98 Nm/deg can be attributed to its ability to facilitate proper rollover, support effective push-off, and maintain a balanced generation of the moment. Moreover, this stiffness is closely linked to optimal stance time, contributing to a more natural gait pattern.

Limitation and future work

This study has several limitations. First, the sample size was relatively small and limited to healthy individuals, which may constrain the generalizability of the results. Second, the walking trials were restricted to level-ground conditions, without evaluating the effects of toe joint stiffness in varied environments such as slopes or stairs. Third, although simulations indicate that the optimal toe-joint stiffness varies across the gait cycle (phase dependent), our experiments evaluated only a fixed-stiffness configuration, which weakens phase-dependent inference and may limit translational releveance to powered assistive devices. Fourth, although the optimization results provide useful insights, the application of these findings in powered systems was not directly tested. while the current framework was shown to be robust to variations in body height, it demonstrated high sensitivity to mass perturbations. The optimization solver failed to converge for both increased and decreased mass conditions relative to the nominal 80 kg. This highlights a limitation in the constraint formulation and trajectory feasibility under altered dynamic loads. Furthermore, although this study aimed to compare simulation and experimental outcomes, we did not conduct a direct numerical comparison due to inherent differences between the computational model and the experimental setup. These differences include simplified representations of body dynamics, joint mechanics, and ground contact modeling. Nevertheless, key qualitative features-such as the progression of toe joint moments and heel-off timing-were found to be consistent.

Future research should expand the participant population and include more diverse locomotor tasks; implement phase-dependent stiffness modulation on hardware and compare it directly with fixed-stiffness baseline; applying the stiffness optimization framework to powered prostheses and exoskeletons to evaluate system-level benefits. Additionally, incorporating multiple optimization criteria-such as Cost of Transport (CoT) and metabolic energy-could offer a more comprehensive evaluation of gait efficiency. Enhancing robustness to dynamic variation, particularly under variable body mass conditions, remains an important direction for future research. Ultimately, these efforts may help translate optimized toe joint designs into wearable robotics that improve mobility, comfort, and long-term user satisfaction.

Conculsion

This study sought to identify an optimal toe joint stiffness value using simulation-based trajectory optimization and to evaluate whether this value aligns with user preference and gait performance in human walking experiments. In simulation, we found that toe joint stiffness is best treated as a time-varying parameter-remaining low during heel-off and rollover to support smooth transitions, and increasing during push-off to enhance propulsion. Although the simulation yielded a time-varying optimal stiffness profile, we selected 0.98 Nm/deg as a representative fixed value by averaging the stiffness during the push-off phase, which plays a critical role in forward propulsion.

In the human walking experiment the 0.98 Nm/deg condition was generally among the most preferred, and the ∞ Nm/deg condition was consistently the least preferred across participants. Taller participants-whose anthropometry closely matched the simulation model-showed the strongest preference for 0.98 Nm/deg, whereas shorter participants showed more varied rankings. Beyond subjective ratings, the 0.98 Nm/deg condition was associated with favorable spatiotemporal metrics, smoother rollover transitions, and balanced moment generation across gait phases.

These findings indicate that moderate toe joint stiffness around 1.04 Nm/deg can improve walking performance and user satisfaction in level-ground walking. While this value may serve as a practical passive stiffness setting for assistive devices without active toe joint actuation, the benefits of time-varying stiffness for powered devices remain to be validated. Future research should extend testing to varied terrains, larger and more diverse participant groups, and hardware implementations of phase-dependent stiffness modulation

to fully assess the translational potential of simulation-optimized stiffness profiles. Thus, while promising, the applicability of these findings to powered prostheses or exoskeletal systems remains to be validated under more diverse and dynamic conditions.

Data availability

The datasets generated and analyzed during the current study are available from github repository. https://github.com/KwonseungCho/Optimizing-Toe-Joint-Experimental-Data

Received: 24 February 2025; Accepted: 28 August 2025

Published online: 26 September 2025

References

- 1. Hughes, J., Clark, P. & Klenerman, L. The importance of the toes in walking. J. Bone Joint Surg. Br. 72, 245-251 (1990).
- 2. Honert, E. C., Bastas, G. & Zelik, K. E. Effect of toe joint stiffness and toe shape on walking biomechanics. *Bioinspiration Biomimet.* 13, 066007 (2018).
- 3. Honert, E. C., Bastas, G. & Zelik, K. E. Effects of toe length, foot arch length and toe joint axis on walking biomechanics. *Hum. Mov. Sci.* 70, 102594 (2020).
- 4. McDonald, K. A. et al. Adding a toe joint to a prosthesis: walking biomechanics, energetics, and preference of individuals with unilateral below-knee limb loss. Sci. Rep. 11, 1924 (2021).
- 5. Hong, W. et al. Empirical validation of an auxetic structured foot with the powered transfemoral prosthesis. *IEEE Robot. Autom. Lett.* 7, 11228–11235. https://doi.org/10.1109/LRA.2022.3194673 (2022).
- 6. Um, H.-J., Kim, H.-S., Hong, W., Kim, H.-S. & Hur, P. Design of 3d printable prosthetic foot to implement nonlinear stiffness behavior of human toe joint based on finite element analysis. *Sci. Rep.* 11, 19780 (2021).
- 7. Patrick, S., Anil Kumar, N., Hong, W. & Hur, P. Biomechanical impacts of toe joint with transferoral amputee using a powered knee-ankle prosthesis. Front. Neurorobot. 16, 32 (2022).
- 8. Teater, R. H., Zelik, K. E. & McDonald, K. A. Biomechanical effects of adding an articulating toe joint to a passive foot prosthesis for incline and decline walking. *PLoS ONE* **19**, e0295465 (2024).
- Rogers-Bradley, E. et al. Variable-stiffness prosthesis improves biomechanics of walking across speeds compared to a passive device. Sci. Rep. 14, 16521. https://doi.org/10.1038/s41598-024-67230-3 (2024).
- Westervelt, E. R., Grizzle, J. W., Chevallereau, C., Choi, J. H. & Morris, B. Feedback control of dynamic bipedal robot locomotion (CRC press, 2018).
- Chao, K. & Hur, P. A step towards generating human-like walking gait via trajectory optimization through contact for a bipedal robot with one-sided springs on toes. In *IEEE/RSJ International Conference on Intelligent Robots and Systems*, 4848–4853, https://doi.org/10.1109/IROS.2017.8206361 (Vancouver, Canada, 2017).
- 12. Chao, K. Bipedal Walking Analysis, Control, and Applications Towards Human-Like Behavior. Ph.D. thesis, Texas A &M University (2019).
- 13. Zarrugh, M., Todd, F. & Ralston, H. Optimization of energy expenditure during level walking. Eur. J. Appl. Physiol. 33, 293–306 (1974)
- 14. Winter, D. A. Biomechanics and motor control of human movement (John wiley & sons, 2009).
- 15. Wächter, A. & Biegler, L. T. On the implementation of an interior-point filter line-search algorithm for large-scale nonlinear programming. *Math. Program.* **106**, 25–57 (2006).
- 16. Kerrigan, D. C., Riley, P. O., Rogan, S. & Burke, D. T. Compensatory advantages of toe walking. Arch. Phys. Med. Rehabil. 81, 38–44 (2000).
- 17. Hansen, A. H., Childress, D. S., Miff, S. C., Gard, S. A. & Mesplay, K. P. The human ankle during walking: implications for design of biomimetic ankle prostheses. *J. Biomech.* 37, 1467–1474. https://doi.org/10.1016/j.jbiomech.2004.01.017 (2004).
- 18. Zelik, K. E. & Adamczyk, P. G. A unified perspective on ankle push-off in human walking. J. Exp. Biol. 219, 3676–3683 (2016).
- 19. Rao, Y. et al. Effects of peak ankle dorsiflexion angle on lower extremity biomechanics and pelvic motion during walking and jogging. *Front. Neurol.* 14, 1269061 (2024).
- 20. Fatone, S., Gard, S. A. & Malas, B. S. Effect of ankle-foot orthosis alignment and foot-plate length on the gait of adults with poststroke hemiplegia. *Arch. Phys. Med. Rehabil.* **90**, 810–818 (2009).
- 21. Schmitthenner, D., Sweeny, C., Du, J. & Martin, A. E. The effect of stiff foot plate length on walking gait mechanics. *J. Biomech. Eng.* 142, 091012 (2020).
- 22. Pongpipatpaiboon, K. et al. The impact of ankle-foot orthoses on toe clearance strategy in hemiparetic gait: a cross-sectional study. *J. Neuroeng. Rehabil.* 15, 1–12 (2018).
- 23. Hebenstreit, F. et al. Effect of walking speed on gait sub phase durations. Hum. Mov. Sci. 43, 118-124 (2015).
- 24. Camargo, J., Ramanathan, A., Flanagan, W. & Young, A. A comprehensive, open-source dataset of lower limb biomechanics in multiple conditions of stairs, ramps, and level-ground ambulation and transitions. *J. Biomech.* 119, 110320 (2021).

Acknowledgements

The authors would like to thank Haewon An, Wooyoung Park, Laeheon Kim, and Sunghwan Bae for their assistance with the experiments. This study was partially supported by Samsung-GIST Intelligent Motor Talent Training Center.

Author contributions

K.C. set up and ran the simulation, set up the experiment, analyzed the results, wrote the original draft, and performed review and editing. K.L. performed writing, review, and editing. P.H. provided project administration, conceptualization, methodology, writing, review, and editing.

Declarations

Competing interests

The authors declare no competing interests.

Additional information

Correspondence and requests for materials should be addressed to P.H.

Reprints and permissions information is available at www.nature.com/reprints.

Publisher's note Springer Nature remains neutral with regard to jurisdictional claims in published maps and institutional affiliations.

Open Access This article is licensed under a Creative Commons Attribution-NonCommercial-NoDerivatives 4.0 International License, which permits any non-commercial use, sharing, distribution and reproduction in any medium or format, as long as you give appropriate credit to the original author(s) and the source, provide a link to the Creative Commons licence, and indicate if you modified the licensed material. You do not have permission under this licence to share adapted material derived from this article or parts of it. The images or other third party material in this article are included in the article's Creative Commons licence, unless indicated otherwise in a credit line to the material. If material is not included in the article's Creative Commons licence and your intended use is not permitted by statutory regulation or exceeds the permitted use, you will need to obtain permission directly from the copyright holder. To view a copy of this licence, visit https://creativecommons.org/licenses/by-nc-nd/4.0/.

© The Author(s) 2025